In situ visualization of organic fouling and cleaning mechanisms in reverse osmosis and forward osmosis

Emily W. Tow[a], Martin M. Rencken[a,b], John H. Lienhard V[a]

[a]*Rohsenow Kendall Heat Transfer Laboratory*
Department of Mechanical Engineering
Massachusetts Institute of Technology
Cambridge, Massachusetts 02139, USA
[b]*University of Pretoria*
Hatfield, 0028 South Africa

Abstract

Fouling models rely on knowledge of foulant accumulation and removal mechanisms. In this study, a fouling visualization apparatus is developed to elucidate centimeter-scale mechanisms of organic fouling and cleaning in reverse osmosis (RO) and forward osmosis (FO). Alginate is used as a model organic foulant and dyed with methylene blue, which is shown not to affect fouling or cleaning, and to sufficiently highlight the gel for visualization at low salinity (up to 1% NaCl). When cleaning by increasing the cross-flow velocity, with or without reverse permeation, foulant peels off the membrane in discrete pieces in both RO and FO. Videos of cleaning show that foulant cake swelling and wrinkling can facilitate gel detachment and removal. Despite their effectiveness in slowing fouling, spacers can hinder removal of detached foulant pieces by obstructing their path. Finally, photographs point to a new mechanism of internal fouling in FO: vapor formation due to sub-atmospheric pressure within the membrane. Awareness of these mechanisms allows for better modeling of fouling and motivates optimization of swelling-inducing cleaning procedures.

Keywords: alginate, desalination, FO, fouling, RO

1. Introduction

Understanding mechanisms of fouling and cleaning in membrane desalination is crucial for improving membrane technology and designing more targeted pretreatment and cleaning strategies. Both low salinity and seawater desalination applications suffer from organic fouling, which includes fouling with gel-forming polysaccharides [1]. Sodium alginate is often used as a model polysaccharide because of its similarity to extracellular polymeric substances (EPS) found in

---

*Address all correspondence to *lienhard@mit.edu*

membrane fouling [2]. Alginate fouling has been studied extensively, particularly in terms of flux decline and cleaning effectiveness, but few studies have investigated mechanisms of foulant removal. Therefore, in this work, we study mechanisms of alginate fouling accumulation and removal in reverse osmosis (RO) and forward osmosis (FO) through both flux measurement and in situ visualization.

Visualization of membrane fouling serves two main purposes: to quantify fouling and to enhance understanding by complementing quantitative measurements. Methods such as nuclear magnetic resonance imaging have been used to measure fouling in situ, but the choice of imaging methods is limited by the materials compatible with the high pressures of RO [3]. Ultrasonic time-domain reflectometry (UTDR) can work through a thick enclosure and has been successfully used to monitor inorganic fouling of RO membranes in situ [3]. Changes in the ultrasonic response of the membrane can be used to calculate foulant thickness [4]. Such quantitative visualization methods have the potential to monitor fouling in real desalination plants, but they have limitations. UTDR, for example, can only provide the foulant thickness at the measurement location, but no information about morphology or patterning. In contrast, qualitative imaging can demonstrate or confirm fouling mechanisms that underlie predictive models.

Several previous studies have used in situ visualization specifically to elucidate mechanisms of fouling and cleaning. Li et al. [5] visually demonstrated the phenomenon of critical flux in microfiltration using latex beads of 3-11.9 μm diameter, while also showing that the critical flux was less pronounced in microfiltration of yeast. Thompson et al. [6] visualized combined biofouling and scaling in RO at pressures up to 25 bar to show that biofouling enhances scaling due to biofilm-enhanced concentration polarization. Microscopic observation of fouling has also been conducted in FO with latex particulates [7], showing that the rapid particle deposition that occurs beyond the critical flux occurs only between the embedded mesh filaments.

In situ visualization of alginate fouling is particularly challenging because the hydrogel formed in the presence of divalent cations is typically clear and, due to its high water content, has a refrac-

tive index close to that of water. Xie et al. [8] captured images of alginate fouling layers formed in FO, pressurized FO, and RO, before and after cleaning, using a polysaccharide-selective fluorescent dye and confocal laser scanning microscopy (CLSM) on samples cut from fouled membranes. The images are used to determine the thickness and quantity of foulant accumulation. However, because the fouled membrane was observed ex situ and the area imaged was less than 1 mm^2, mechanisms of fouling and cleaning that are only observable during operation or that occur over macroscopic areas could not be identified. In this work, we highlight alginate fouling on FO and RO membranes with methylene blue and observe the membranes in situ to identify centimeter-scale fouling and cleaning mechanisms.

By visualizing alginate fouling in situ without magnification, this study identifies several previously undocumented mechanisms of flux decline and foulant removal: Osmotic backwashing leads not to gel dissolution, but the sloughing of macroscopic chunks. Gel swelling and wrinkling due to changes in ionic composition are powerful drivers of gel delamination and removal. Feed spacers, though effective at slowing flux decline, can reduce cleaning effectiveness by impeding removal of gel pieces. Finally, in FO with membranes oriented in PRO mode, increased membrane reflectance points to vapor formation due to low pressure within the membrane.

2. Experimental methods

Membranes are fouled with dyed alginate during RO and FO operation while transmembrane flux and photographs or videos are recorded. Methylene blue is used to dye the alginate and enable visualization of the deposition and removal of this otherwise clear gel. Cleaning steps are performed to elucidate foulant removal mechanisms.

2.1. Apparatus

Fouling and cleaning of RO and FO membranes are performed in a plate and frame membrane module. Pressure, temperature, and flow rate are controlled while permeate mass (or draw mass,
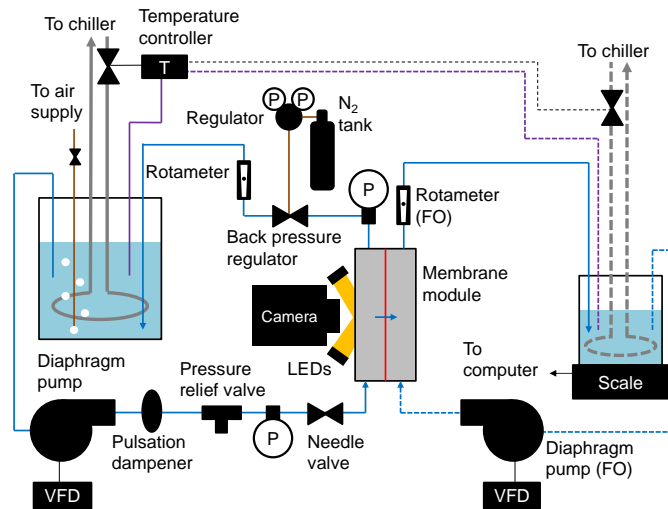
Figure 1: Schematic diagram of experimental fouling visualization and flux measurement apparatus that can be operated as RO or FO. Dashed lines represent flows only present in FO operation. VFD stands for variable frequency drive. Figure adapted from our previous report [9].

in FO) is recorded, as detailed in our previous report [9]. A camera records fouling and cleaning through a window in the membrane module. Figure 1 shows the experimental apparatus.

Flux in lmh (L/m^2-hr) is calculated from the change in permeate volume over 15 minute intervals and the active membrane area. The mass of permeate or draw is recorded every second with an Ohaus Scout Pro digital scale, which has a capacity of 6 kg and a repeatability of 0.1 g, and RealTerm software. In RO, permeate enters the tank through a rigid 1/8 in. (3.2 mm) tube submerged in the liquid, which displaces a negligible volume. In FO experiments, the volume displaced by the immersed cooling coil, draw inlet, and draw outlet is accounted for in the data analysis.

2.2. High pressure fouling visualization module

The module that holds the membrane is designed to withstand high pressure (up to 69 barg) and enable viewing of the membrane surface. For the module body, 316 stainless steel was chosen for its corrosion resistance. Polycarbonate was chosen as the material for the portal for its water tolerance, strength, and machinability. Figure 2 shows a rendering of the membrane module.

Inside the membrane module, the feed channel is cut 1 mm deep to approximate flow condi-
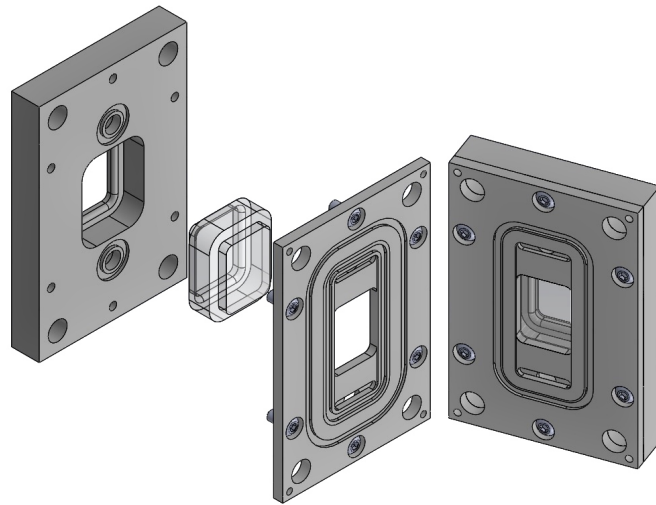
4

Figure 2: CAD rendering of the high pressure fouling visualization module with the feed side disassembled.

tions in spiral-wound RO elements. The draw/permeate channel is also 1 mm deep. The channels are 8 cm long and 3 cm wide. Manifolds were designed to minimize entrance/exit effects. In RO operation, the draw/permeate channel contains five layers (for a total thickness of 1 mm) of permeate spacer mesh from a low pressure RO module. In FO operation, a 0.79 mm-thick, non-woven mesh feed spacer (Sterlitech 31 mil diamond) is used in the draw channel. The feed channel is left empty to encourage fouling except in three trials, in which either a coarse feed spacer identical to the draw spacer or a fine feed spacer (0.43 mm thick, Sterlitech 17 mil diamond) is placed in the feed channel.

The transparent polycarbonate portal shows the full width of the membrane but only the middle 4 cm in the length direction. The polycarbonate sits flush with the metal on the channel side so that the flow is not disturbed. The membrane is illuminated from the feed side using two white LED arrays placed on either side of the camera, each illuminating the opposite half of the membrane. (Back-lighting the fouled membranes was also attempted, but the image quality was inferior.) Unlike RO membranes, the FO membrane is translucent, so white paper is placed on draw side window in FO operation to block light from behind the module.

O-ring grooves were designed to seal against high pressures while minimizing force on the

membrane. Design details are included to enable replication. Three concentric O-rings (nitrile rubber in size 3/32) seal the module halves to each side of the membrane and to each other. Unlike some commercial membrane modules, the cross-sectional area of each O-ring is just 75% that of the the groove. The groove depth is 65% of the O-ring cord diameter. The gap outside the grooves is limited to 50 μm to prevent O-ring extrusion at high pressure. As a result, the module can be pressurized to at least 69 bar without leaking and the membrane damage by the O-rings is limited, as demonstrated by the closeness of measured RO salt rejection to membrane specifications [9].

2.3. Membranes

High-rejection thin-film composite polyamide membranes (Dow FILMTEC SW30HR) are used in RO tests. For FO tests, asymmetric cellulose triacetate (CTA) membranes with a woven support layer (Hydration Technology Innovations) are used in FO mode (active layer facing the feed) except where noted. The RO membrane has a permeability of approximately 3×10^{-12} m/s-Pa to 4.4×10^{-12} m/s-Pa according to the included specifications. In our previous report [9], the FO membrane was shown to have a water permeability of 1.9×10^{-12} m/s-Pa, support layer structural parameter of 5.7×10^{-4} m, and support layer dispersivity (which describes the enhancement of diffusion by convection through the porous support) of 1.65×10^{-4} m. Salt permeation coefficients of 2.38×10^{-8} m/s in RO and 5.32×10^{-8} m/s in FO and were calculated from membrane specifications to avoid measurement error resulting from the small size of our membrane module and the potential for salt leakage at the edges.

2.4. Feed and draw solutions

Sodium alginate is used as a model organic foulant at a concentration of 200 mg/L in all trials. Sodium alginate (Sigma-Aldrich A2033, denoted by "alginate" from here on) is a polysaccharide with a molar mass of 80,000-120,000 g/mol (as indicated on the supplier website). In all trials, 1 mM calcium chloride is added to the prepared feed solution to initiate fouling through complexation with the polyguluronates in alginate (see, e.g., [10, 11, 12]). Due to this complexation and

the convection of solutes toward the membranes during operation, the alginate forms a hydrogel on the membrane.

Methylene blue (Alfa Aesar), a monovalent cationic dye, is used to dye the foulant. At sufficiently low salt concentrations, it colors the gel more intensely than the feed solution. Concentration of dye in the gel layer by cake-enhanced concentration polarization (see, e.g., [13]) also contributes to foulant layer visibility. Concentrated (1% wt.) methylene blue is added to the feed solution during membrane equilibration to reach a concentration of 7.6 μM.

Sodium chloride (Alfa Aesar 99% min.) is used in the feed and draw solutions. D-(+)-glucose (Alfa Aesar 99% min., denoted as "dextrose" in what follows) is also used to raise the feed osmotic pressure in one trial. Sodium chloride concentration is determined with a Hach conductivity meter and interpolation of tabulated NaCl conductivity data in Ref. [14]. Deionized water is used as the solvent throughout this experiment to prevent membrane damage by the chlorine in tap water. The draw solution is degassed before use to minimize outgassing, which displaces draw and affects the flux measurement. The feed solution is not degassed, but the membrane module is oriented vertically with upward flow to prevent air accumulation.

2.5. Fouling and cleaning procedure

Membranes are equilibrated and compacted as detailed in our previous report [9] before the concentrated alginate and calcium chloride solutions are sequentially added. To minimize differences in fouling rate and cleaning effectiveness due to variations in flux, the initial flux before fouling is kept as close as possible to 23 L/m^2-hr (lmh) by choosing the feed pressure in RO and the draw solution's concentration in FO. In all trials, the feed cross-flow velocity is 8.3 cm/s during fouling and 25 cm/s during cleaning. After approximately eight hours of fouling, the cleaning step is performed for one hour (except where noted). Cleaning is either performed with forward flux, which only involves increasing the cross-flow velocity, or with reverse flux, which also involves reducing the feed pressure to atmospheric in RO or replacing the saline draw solution with deionized water in FO.

7

A Nikon P530 camera captures photographs every 30 seconds during fouling and videos during cleaning. The camera is manually focused on the membrane at the beginning of each experiment.

2.6. Data analysis

Flux decline (given in Sec. 4 as normalized flux) quantifies the response of a membrane and process to fouling. Normalized flux is calculated as a ratio of measured flux to the flux that would be predicted for an unfouled membrane under the same conditions. As in past studies (e.g., [15]), feed and draw concentrations are allowed to change gradually as water crosses the membrane. Here, these changes are accounted for in the prediction of foulant-free flux. Foulant-free predictions are made using the foulant-free models for RO and FO in [9], which are comparable to standard models except for the addition in [9] of dispersive salt transport in the FO support layer. The 95% confidence interval for flux decline for the present experimental apparatus operating at the same initial flux range is ±0.036 in RO and ±0.054 in FO [9].

Photographs and videos are used to identify mechanisms of fouling and foulant removal that have not been observed previously. Where noted, the contrast of individual colors was adjusted in MATLAB to improve clarity, but these adjustments were uniform within each image and throughout each video or set of images.

3. Validation of visualization method

3.1. Foulant visibility

To validate the visualization method, we first test the ability of methylene blue to dye alginate foulant in saline solutions. Ideally, as a layer of alginate gel forms, the cationic dye should preferentially bind to the negatively-charged alginate gel over the dilute alginate solution. However, other cations compete with the dye. Figure 3 shows video stills of fouled RO membranes during cleaning at two NaCl concentrations. As in all trials reported on here, the feed contains 1 mM $CaCl_2$ and 200 mg/L alginate. In Fig. 3a, the sodium concentration in the feed is 0.17 M, and it
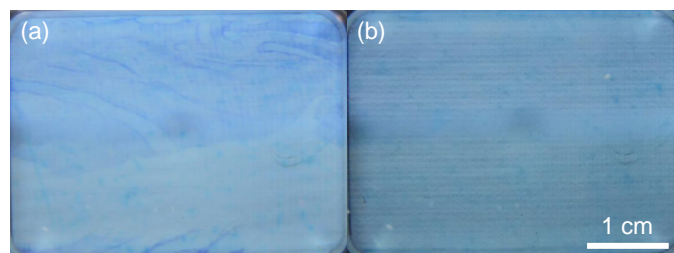
8

Figure 3: Video stills of alginate gel cakes with methylene blue on RO membranes during cleaning with 1 mM $CaCl_2$, 200 mg/L alginate, and (a) 0.17 M NaCl and (b) 0.52 M NaCl.

is possible to make out edges where the gel sheet has torn off as well as wrinkles in the sheet. In Fig. 3b, the NaCl concentration is three times as high, and although the image is uniformly blue because of the dye in the feed solution, no edges are visible. As we will show, digitally enhancing contrast improves visibility when there is contrast to begin with, but it appears that methylene blue is not able to dye alginate foulant at high salinity (e.g., seawater salinity). For high salinity studies, it may be worthwhile to test the visibility of alginate gel with other cationic dyes such as thionine acetate and pinacyanol chloride. For now, we will limit the scope of our investigation to fouling and cleaning at relatively low salt concentrations that might be found in brackish water desalination.

3.2. Effect of dye on fouling rate and reversibility

To demonstrate the viability of methylene blue for fouling visualization, we next confirm that a low concentration of the dye does not affect fouling rate or susceptibility to cleaning. RO fouling and cleaning trials with the same initial flux and the same feed solution with and without methylene blue are compared in Fig. 4. Figure 4a shows the flux decline in both trials, from which it appears that methylene blue inhibits fouling. However, permeability varies between membrane samples, as evidenced by the different pressures needed to achieve the same initial flux (39 barg for the trial with dye and 27.3 barg for the trial without). Membrane permeability has been shown by the layered membrane model developed in our previous report [9] to affect flux decline for a given amount of foulant accumulation. In both cases, cleaning at atmospheric pressure with high cross-
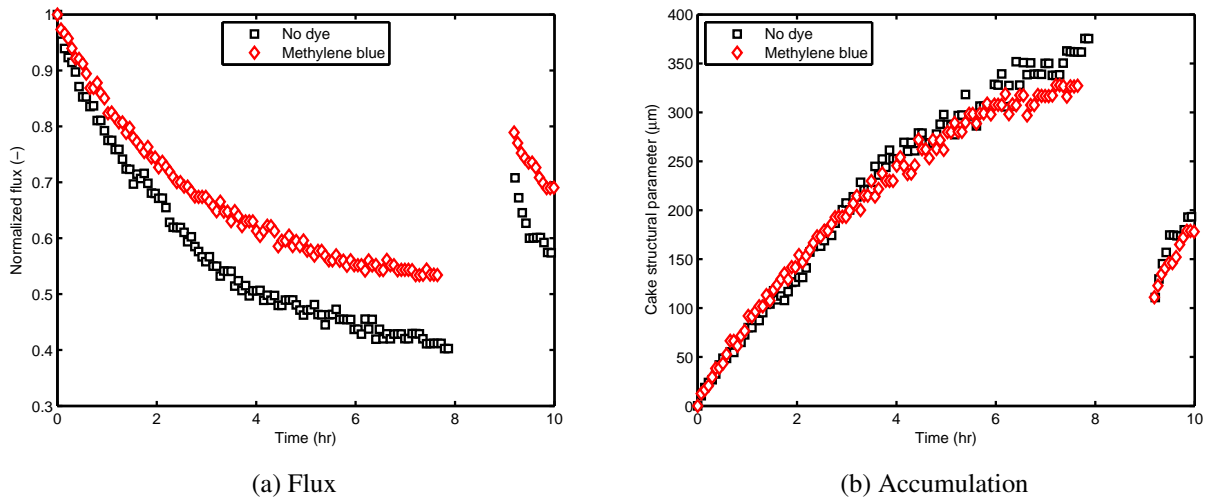
9

Figure 4: (a) Flux decline and (b) foulant accumulation in RO with 0.17 M NaCl, 1 mM CaCl$_2$, and 200 mg/L alginate, with and without methylene blue dye, at feed pressures of 39 and 27.3 barg, respectively. Initial flux was 21.7±0.2 lmh. No feed spacer was used. Gap in data indicates mechanical cleaning at atmospheric pressure. Uncertainty in normalized flux is ±0.036 and uncertainty in structural parameter is ±60 μm at the end of the fouling step.

flow velocity (25 cm/s) for one hour partially restores the flux, but it is difficult to claim that the cleaning step was equally effective in the two cases.

To isolate the effect of the dye from the effect of varying membrane permeability, the foulant accumulation rate and cleaning effectiveness are compared by analyzing the cake structural parameter using the layered model of transport in fouled RO membranes presented in our previous report [9] (summarized in Appendix A). Figure 4b shows that the cake structural parameter (the effective foulant thickness, Eq. A.1), which is approximately equal to the actual thickness of accumulated gel because of the high porosity and low tortuosity typical of alginate gels [16], increases almost identically in the two trials to an effective thickness of about 350 μm. After cleaning, the effective cake structural parameter ("effective" because the remaining foulant layer is uneven and/or detached from the membrane) returns to approximately the same value, which shows that the dye does not substantially affect the susceptibility of the foulant to cleaning. We conclude that methylene blue does not affect foulant accumulation or removal and is therefore a suitable dye for

10

visualization studies at low salinity.

4. Results

4.1. Swelling detachment mechanism

In some trials, swelling and wrinkling of the foulant were observed prior to complete detachment. This phenomenon, which occurred in both RO and FO, has the potential to be leveraged in membrane cleaning protocols.

To visualize mechanisms of foulant removal at high pressure, a feed solution of 0.17 M NaCl, 0.58 M dextrose, 1 mM $CaCl_2$, and 200 mg/L alginate was subjected to RO at a feed pressure of 69 barg. Dextrose was used to raise the osmotic pressure because, as shown in Fig. 3, methylene blue does not sufficiently dye the foulant gel at high sodium chloride concentrations. After fouling, the pressure was reduced to atmospheric, and the feed pump was stopped so that the foulant could be filmed undisturbed. This video is provided in the supplementary materials; several frames are highlighted in Fig. 5. Figure 5a shows that the foulant layer wrinkles in response to the reduction in pressure and Fig. 5c-e show the subsequent removal of the foulant layer when the cross-flow velocity is increased to 25 cm/s. Initially, many small wrinkles form across the membrane, mostly aligned with the texture of the membrane that results from pressing against the permeate spacer. As the wrinkles grow, some join while others disappear, indicating that the gel sheet is detaching from the membrane. By the time the cross-flow velocity is increased, the sheet is almost completely detached. However, the edges of the foulant are still attached due to edge effects in the small membrane module, so the gel sheet flaps in the flow until it tears. Large sections of the gel sheet are then torn away.

Gel swelling and wrinkling as a precursor to detachment of the entire gel sheet was also seen in an FO trial with cross-flow during cleaning. In this trial, foulant was accumulated in FO orientation (feed facing the active layer, denoted as "FO mode" hereafter) using a 4.8 M NaCl draw solution and a feed of 0.17 M NaCl, 1 mM $CaCl_2$, and 200 mg/L alginate at 8.3 cm/s with no feed spacer.

11

Cleaning with reverse permeation was performed by replacing the draw solution with tap water and increasing the feed velocity to 25 cm/s. Despite the high cross-flow velocity, which was absent during most of the wrinkle growth in the RO test described above, one wrinkle formed after two minutes of cleaning and grew for approximately six seconds before the entire gel sheet detached from the active area of the membrane. However, the sheet was still pinned at the edges of the channel, as it was in the RO trial above, and it peeled off 37 seconds later. Figure 5e-g shows the wrinkling and detachment of the gel sheet in FO.

Wrinkle formation can be explained by isotropic swelling of the gel when the direction of permeation is reversed. Swelling leads to wrinkling when the elastic energy of the swollen gel, which is under compression in the plane of the membrane to which it is attached, is enough to overcome adhesion to the membrane. The proposed mechanism is illustrated in Fig. 6. A similar wrinkling instability forms when a thin film under compressive stress is adhered to a thick substrate [17], in which case thicker films with a lower adhesion energy are more prone to wrinkling.

The swelling itself can be explained by the change in ion concentration in the gel layer when the pressure is released during cleaning in RO or the draw solution is changed in FO. Although it has been proposed that pressure itself compacts alginate gels, this is only physically explained if alginate is compressible, which measurements show that it is not [8]. Additionally, the formation of wrinkles during cleaning of the FO membrane in Fig. 5 cannot be explained by a decrease in pressure. However, the reduced pressure during RO cleaning and reduced draw solution concentration during FO cleaning both cause water to flow back through the membrane into the feed by osmosis[1]. Whereas during fouling, concentrative cake-enhanced concentration polarization caused the ion concentration in the gel to exceed that of the feed, reverse water permeation by osmosis during the cleaning step causes dilutive concentration polarization in the gel layer and ion concentration in the gel becomes lower than that of the feed. In addition, the lower diffusion coefficient of calcium chloride causes the sodium:calcium mole ratio to increase when the concentration polar-

---

[1]This is sometimes termed "osmotic backwashing," particularly when the feed concentration is increased.
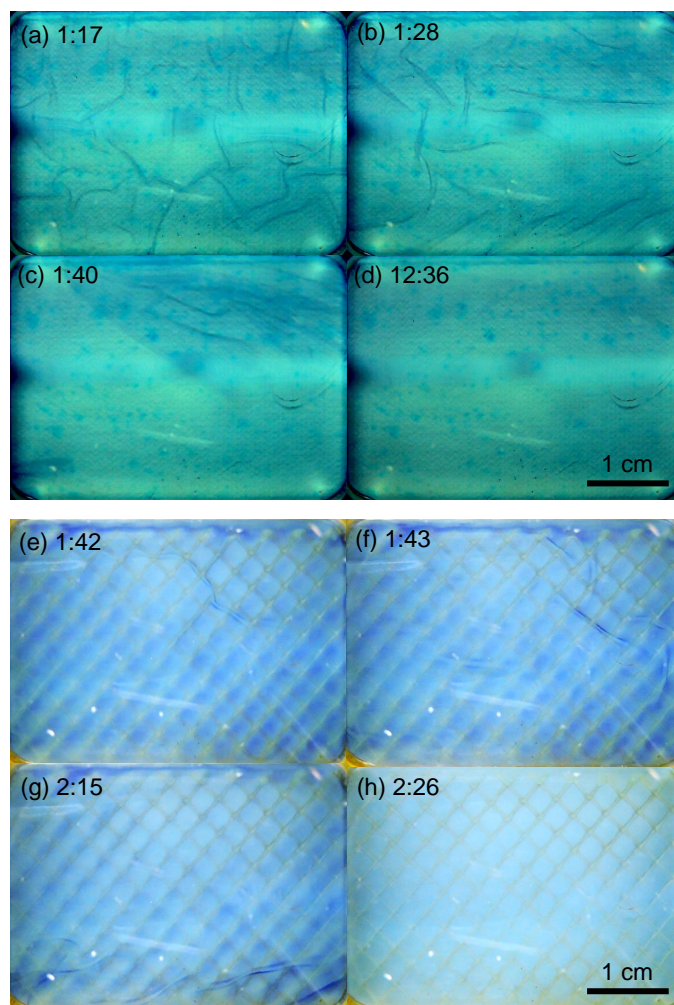
Figure 5: Video stills of wrinkle formation during cleaning of (a-d) RO and (e-h) FO membranes without feed spacers. Feed contained 0.17 M NaCl, 1 mM $CaCl_2$, and 200 mg/L alginate, plus 0.58 M dextrose in the RO trial. RO fouling was performed at a feed pressure of 69 barg. In the RO trial, feed pressure was gradually reduced to atmospheric during the period -0:55 to 0:00 and held at 0 barg thereafter. Feed velocity was reduced from 8.3 cm/s (left to right) to 0 cm/s from 0:18 to 0:22, held at 0 cm/s until 1:27, raised to 25 cm/s between 1:27 to 1:32, and maintained a 25 cm/s thereafter. (a) Wrinkles begin to form under stagnant conditions. (b) As the velocity is increased, the wrinkled sheet deforms with the flow. (c) Partially-cleaned membrane with gel remaining in the upper-right section. (d) The cleaned membrane. In the FO trial (e-h), fouling was performed with a draw solution of 4.8 M NaCl and a coarse draw spacer. Cleaning was performed with 25 cm/s feed cross-flow and tap water in the draw channel. (e) Wrinkles form in the upper-right quadrant. (f) The sheet detaches and wrinkles migrate downstream. (g) The detached sheet is pinned at the edges of the channel. (h) The cleaned membrane. Image contrast was enhanced uniformly within (a-d) and (e-h). Time stamps are in minutes and seconds beginning at the start of cleaning.
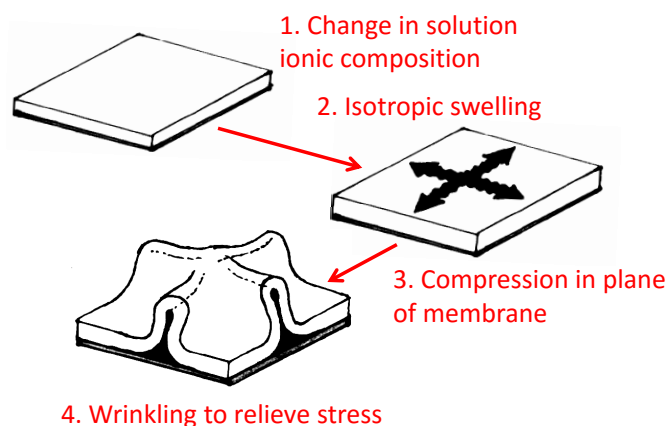
Figure 6: Proposed mechanism of foulant gel wrinkling and detachment.

ization in the gel is switched from concentrative to dilutive.[2] Moe et al. [18] show that alginate gels in sodium chloride solutions swell when the concentration in the surrounding fluid is decreased, which is consistent with the swelling seen in Fig. 5. However, the same study shows that alginate gels in calcium chloride solutions exhibit hysteresis: although they shrink when the concentration is increased, they do not re-swell when the concentration is decreased because bound calcium ions are not released. However, gels in mixed Na–Ca–Cl solutions may exhibit less hysteresis than those in pure $CaCl_2$ solutions because of the ion-exchange reaction [10] between bound calcium and sodium in alginate gels. Further research is needed in this area to fully characterize and manipulate the foulant gel swelling phenomenon. However, our preliminary experiments in alginate gel swelling indeed show that gel volume increases with decreasing ionic strength and also increases with increasing sodium:calcium mole ratio.

Swelling helps remove alginate fouling by instigating detachment of the gel from the membrane and lowering the energy barrier to foulant removal. Swelling by introduction of calcium-free sodium chloride solutions has previously been reported to cause alginate fouling removal [19]. In the absence of visual observations, the removal mechanism after introduction of a more

---

[2]In FO, the ionic strength still decreases, but the sign of the change in sodium:calcium ratio depends to some extent on the draw solute and membrane solute permeation coefficient.

concentrated NaCl feed solution was theorized to be swelling of the gel, dissolution of the gel by breaking the bonds between calcium and alginate, and finally "layer-by-layer removal" of the foulant by "mass transfer" [19]. However, at least in the present study, it is clear that alginate gel removal occurs not by diffusion but by the release of macroscopic sheets. The present observations suggest that cleaning processes can be designed to instigate foulant layer detachment and rapid, macro-scale removal by including a step designed to cause swelling of the foulant.

4.2. Effects of feed spacers

To investigate the effect of feed spacers on foulant deposition and removal, RO and FO trials were conducted with and without feed spacers. The feed spacers used are described in Sec. 2.2. Although feed spacers do reduce the rate of flux decline, we find that they also reduce the cleaning effectiveness by impeding the flow of detached foulant pieces.

Figure 7 shows the fouled RO membrane with the coarse and fine feed spacers. The standard feed solution of 0.17 M NaCl, 1 mM $CaCl_2$, and 200 mg/L alginate was used. The pattern of fouling is less uniform with the coarse spacer than without a spacer (e.g., Fig. 5a). The color is generally darker between the filaments of the spacer, but the intensity also varies across the membrane, suggesting that the spacer (which is 0.21 mm narrower than the channel) did not lay flat. This spatial variability highlights the complexity of spacer design for fouling control: minute changes in spacer geometry can affect fouling. Unfortunately, the foulant visibility with the fine spacer is poor and the presence of either feed spacer makes it difficult to detect the edges of the foulant and see what occurs during cleaning. Photos of the cleaning process are therefore not included here.

Changes in RO flux due to fouling and cleaning with and without spacers are shown in Fig. 8. Flux decline is most severe in the case with no spacer, and similar between cases with different spacers. After cleaning at atmospheric pressure, the flux recovers to roughly the same level for all three cases, although the fractional flux recovery is better without the spacer.
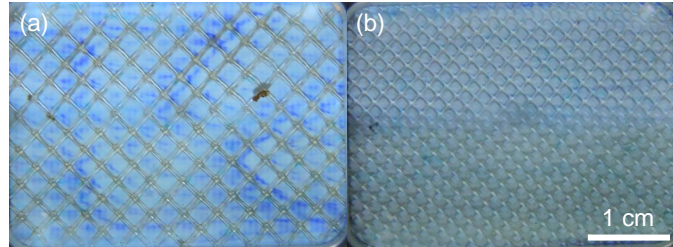
Figure 7: Photographs of the fouled RO membrane with (a) coarse and (b) fine spacers.
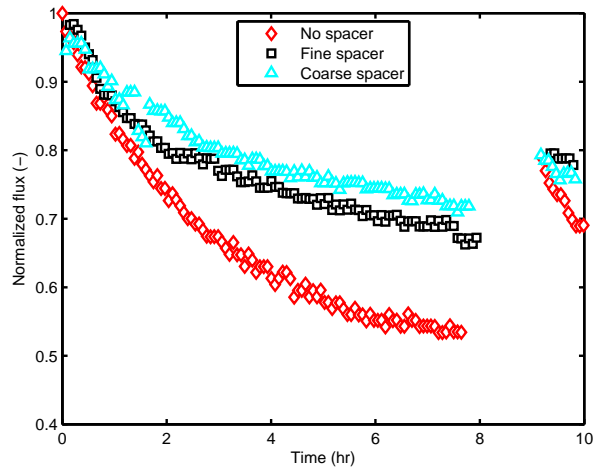

Figure 8: Flux decline in RO with fine, coarse, and no feed spacer at feed pressures of 35.2, 37.5, and 39 barg, respectively. Feed contained 0.17 M NaCl, 1 mM $CaCl_2$, and 200 mg/L alginate and initial flux was 21.5±0.6 lmh. Gap in data indicates mechanical cleaning at atmospheric pressure. Uncertainty in normalized flux is ±0.036.
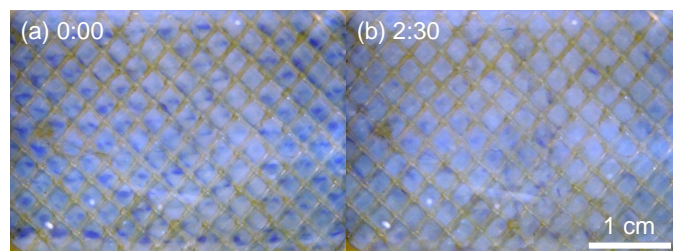
16

Figure 9: Video stills of fouled FO membrane with a coarse feed spacer (a) before and (b) during cleaning with 25 cm/s cross-flow velocity and tap water draw.

Figure 9 shows the spatial pattern of fouling in an FO trial with an identical feed solution to the RO trials shown in Figs. 7 and 8. Foulant is more visible than in the RO cases, and a change can be clearly seen during the first 2.5 minutes of cleaning. Before cleaning, the pattern of the fine draw spacer behind the membrane is visible, suggesting that draw spacer design can influence fouling patterns through their effect on the spatial variation in draw-side mass transfer coefficient and transmembrane flux.

During cleaning, the gel detaches from the membrane, but its movement through the channel is hindered by the presence of the spacer. A video of this cleaning process, from which the stills in Fig. 9 are taken, is provided in the supplementary materials. Because the macroscopic pieces of detached gel are prevented from flowing downstream by the diamond spacer, they instead move diagonally, tangent to one set of spacer filaments. Once enough gel travels in this way and accumulates at the edge of the channel, some of it changes direction and moves diagonally tangent to the other set of spacer filaments. As shown in Fig. 10, the result is a very low cleaning effectiveness similar to that seen with the same spacer in RO under similar conditions in Fig. 8. In contrast, in the case of FO with no spacer, the cleaning step was only run for 15 minutes because it was clear that the entire sheet of foulant had been removed[3].

Figures 8 and 10 show that, in both FO and RO fouling, spacers reduced flux decline but also

---

[3]In fact, it came off in one piece and clogged the downstream back pressure regulator, causing the feed pressure to climb to 2 barg temporarily. The pressure spike may have stretched the membrane, which would explain why the normalized flux slightly exceeded 1 after cleaning.
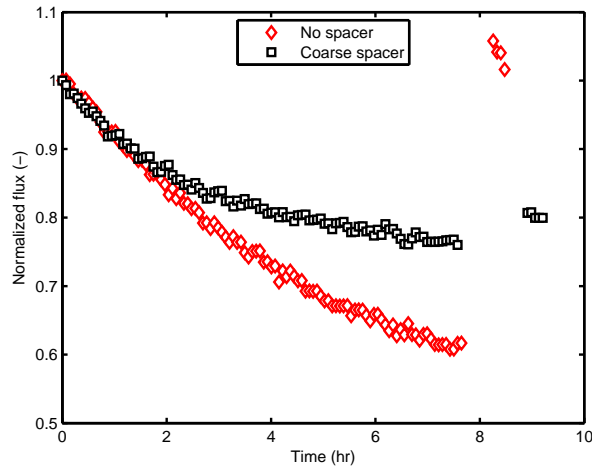
Figure 10: Flux decline in FO (FO mode) with and without a coarse feed spacer at draw concentrations of 4.9 and 4.8 M NaCl, respectively. Feed contained 0.17 M NaCl, 1 mM CaCl$_2$, and 200 mg/L alginate and initial flux was 25.1 lmh in both cases. Draw velocity was 4.3 cm/s in the trial with a feed spacer and 16.7 cm/s in the trial without. In the case with no spacer, cleaning was stopped after 15 minutes because it was clear that the entire foulant layer had been removed.

reduced the fraction of the flux decline recovered by cleaning. Clearly, spacers can improve the fouling resistance of RO and FO systems, but spacers used in systems with gel-forming foulants should ideally be designed to minimally impede the flow of foulant pieces once those pieces are detached from the membrane.

4.3. Effect of permeation direction on cleaning

Flux recovery and foulant removal are affected by the direction of permeation during cleaning. In this study,the direction of permeation during RO cleaning is determined by the feed pressure: for forward-flux cleaning, the pressure is maintained so that permeation continues as usual; for reverse-flux cleaning, the feed pressure is reduced to atmospheric, causing permeate to flow by osmosis back into the saline feed. Cleaning with reverse permeation was found to be more effective at removing foulant and recovering flux.

Figures 11 and 12 show video stills from cleaning fouled RO membranes with forward and reverse permeation, respectively. As the cleaning step progresses, different processes govern foulant
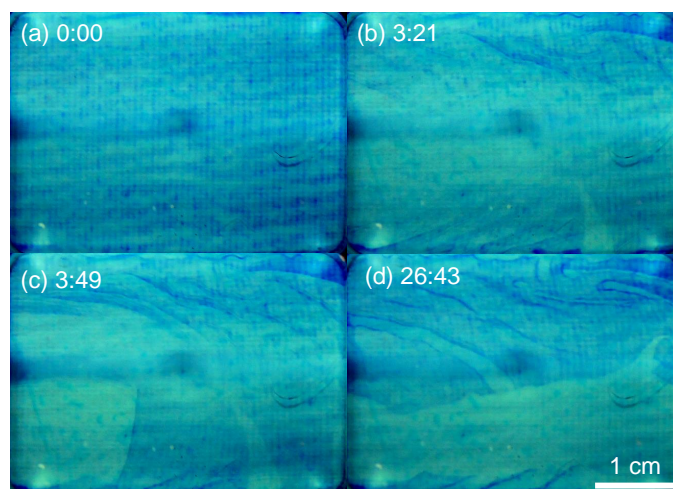
18

Figure 11: Video stills of cleaning an RO membrane at high feed pressure (35 barg) with a feed of 0.17 M NaCl, 1 mM $CaCl_2$, and 200 mg/L alginate. Contrast was enhanced uniformly. (a) is the fouled membrane before cleaning, which shows the pattern of the spacer. In (b), the foulant cake wrinkles in the upper right and tears in the lower right corner when the membrane is subjected to cross flow; (c) shows further wrinkling and tearing. (d) shows the state of the cake at 26 minutes, which does not change significantly during the rest of the hour of cleaning.

removal depending on the direction of permeation. When the foulant cake detaches from the membrane during forward permeation, cake-enhanced concentration polarization is reduced because solute flow is no longer confined to the direction perpendicular to the membrane, resulting in lower concentration of methylene blue. The lighter color in Fig. 11b suggests that the gel sheet has separated from the membrane in the case with forward permeation. The gel appears to bend in the direction of flow, forming wrinkles along the sides of the channel and tearing in multiple places. Eventually, a large section of the gel sheet tears off and flows away. The majority of the sheet remains in place for the remainder of the cleaning step. The detachment of the gel sheet cannot be explained by swelling or shrinking of the gel, because the ionic environment was not changed; the actual cause remains unclear.

Figure 12 shows the progression of the cleaning step when the direction of permeation is reversed by reducing the feed pressure to atmospheric. As in Fig. 11, the initial reduction in color intensity can be attributed to reduced concentration polarization of the dye in the gel, but in this case the flow of dye is back toward the feed because the direction of permeation is reversed.
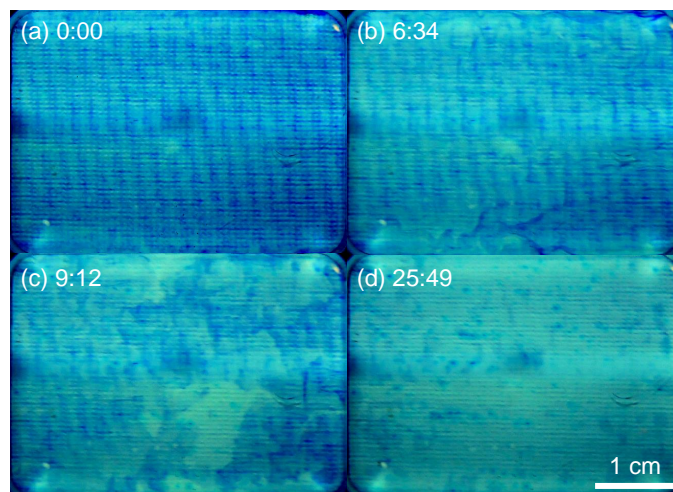
19

Figure 12: Video stills of cleaning an RO membrane at atmospheric pressure. The feed, which was pressurized to 39 barg during fouling, contained 0.17 M NaCl, 1 mM $CaCl_2$, and 200 mg/L alginate. Image contrast was enhanced uniformly. (a) shows the fouled membrane before cleaning. (b) shows some wrinkling of the cake near the edges; (c) shows further wrinkling and patches where the gel has been removed. (d) shows the state of the membrane at 26 minutes, which does not change significantly during the rest of the hour of cleaning.

Gradually, small wrinkles form, and then pieces of gel break off and are removed with the flow.

Figures 13 shows that the cleaning step with reverse permeation was more successful. Cleaning involving reverse permeation ("backwashing") is common, and the improvement is typically attributed to the change in direction of drag force on the porous cake [20]. However, the relationship between permeation direction and foulant removal effectiveness is not entirely straightforward. One study showed that osmotic backwashing in FO was effective at removing alginate gel or silica nanoparticles, but not humic acids [20]. In the salt cleaning experiments of Lee and Elimelech [19], better RO flux recovery when cleaning with NaCl solutions was achieved with a high forward permeation rate of 20 μm/s than when reverse permeation was allowed. The salt solution was then forced into the foulant layer and concentrated there by cake-enhanced concentration polarization. In both the Lee and Elimelech study and the present comparison, regardless of the pressure or direction of permeation, the cleaning step was more effective when the change in the ionic environment of the alginate gel was larger.
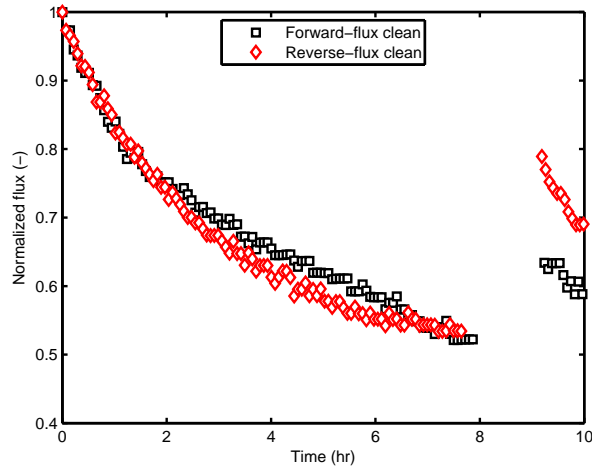
20

Figure 13: Normalized flux in RO with 0.17 M NaCl, 1 mM CaCl$_2$, and 200 mg/L alginate with forward-flux cleaning at RO pressure and reverse-flux cleaning at atmospheric pressure, each beginning at 8 hours. RO feed pressures were 35 and 39 barg, respectively. Initial flux was 21.6±0.3 lmh. Gap in data indicates cleaning. Uncertainty in normalized flux is ±0.036.

4.4. Effect of FO membrane orientation

The cleaning mechanisms observed thus far (wrinkling, peeling, hindrance by spacers) have been identical between FO and RO trials with the feed facing the active layer. The typically higher susceptibility to cleaning of FO has previously been attributed to a looser foulant layer formed in the absence of "compaction" by hydraulic pressure [21], but the present results do not indicate that cleaning proceeds differently in FO and RO. However, we have identified one previously undocumented mechanism of fouling that is unique to FO membranes in PRO orientation (feed facing the support layer, denoted as "PRO mode" hereafter). The PRO mode is important to consider because it achieves higher flux in applications with low-concentration feeds, such as personal hydration packs and fertigation, and yet is often avoided because of its typically worse fouling propensity [22]. In this section, we present evidence of vapor formation inside the FO membrane in PRO mode.

Alginate fouling in forward osmosis (both FO mode and PRO mode) with a feed NaCl concentration of 0.17 M is shown over time through unaltered photographs in Fig. 14. In the FO mode

21

test, the draw solution was 4.8 M and the initial flux was 25.1 lmh. In the PRO mode test, the draw solution was 4.1 M and the initial flux was 23.6 lmh. In both cases, there is no feed spacer and a coarse draw spacer is used with a draw solution velocity of 16.7 cm/s. In FO mode (Fig. 14a-c), fouling results in almost no visible change despite the significant flux decline shown in Fig. 15. In PRO mode (Fig. 14d-f), the image begins almost uniformly blue except for a few patches of lighter blue with with a faint texture of the woven support layer, whose fibers are around 100 μm apart [23]. These pale patches appear to indicate regions where the support layer is not fully wetted, causing reflections from inner air–water or air–polymer interfaces. After five hours of fouling (Fig. 14b), the total area of the pale regions has increased. By eight hours (Fig. 14c), the pale regions cover a significant fraction of the membrane, and the texture of the woven support layer is clearly visible in those regions. It appears that, in PRO mode, parts of the membrane are drying out. This claim is discussed later in this section.

In Fig. 15, flux decline rates are compared between FO membranes in FO and PRO modes as well as RO membranes fouled under similar conditions. In RO and FO-mode FO, flux declines in a similar shape toward what appears to be a similar asymptote, but the FO flux decline is slower. As explained in Ref. [24], FO flux decline is mitigated by the balancing effect of internal concentration polarization (ICP). Because of this effect, termed "ICP self-compensation" [24], FO flux is expected to decline more slowly, especially in FO mode because the support layer is facing the more concentrated draw. FO flux decline is expected to be greater in PRO mode than in FO mode because of the more pronounced ICP self-compensation effect when the support layer is facing the draw. However, PRO-mode flux decline is not expected to be greater than in RO, as it is shown to be in Fig. 15, unless there are additional mechanisms of flux decline unique to PRO-mode FO. Enhanced flux decline in PRO mode over FO mode has previously been attributed to the smaller ICP self-compensation effect and pore clogging by foulants [25], but this visualization study shows that internal fouling due to vapor formation may be an additional driver of flux decline in PRO mode.
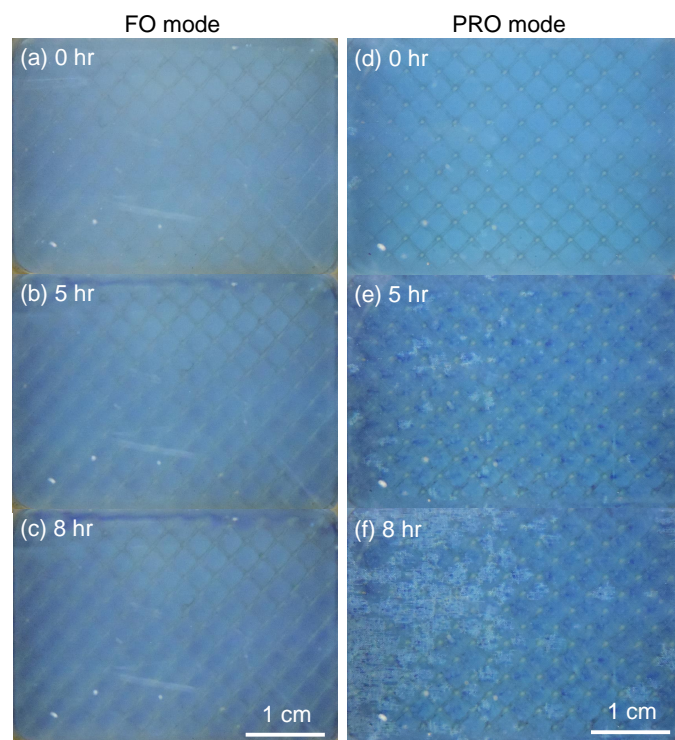
Figure 14: Photographs of FO membrane during fouling in FO mode and PRO mode with a feed of 0.17 M NaCl, 1 mM $CaCl_2$, and 200 mg/L alginate with no feed spacer (the draw spacer is visible through the membrane). Fouling in FO mode (a-c) is barely visible, indicating relatively uniform accumulation. Before fouling in PRO mode, the image (d) is uniformly blue, except for a few lighter patches. In (e) and (f), fouling has resulted in expansion of the lighter regions, which are interpreted as area where air or vapor has accumulated in the membrane.
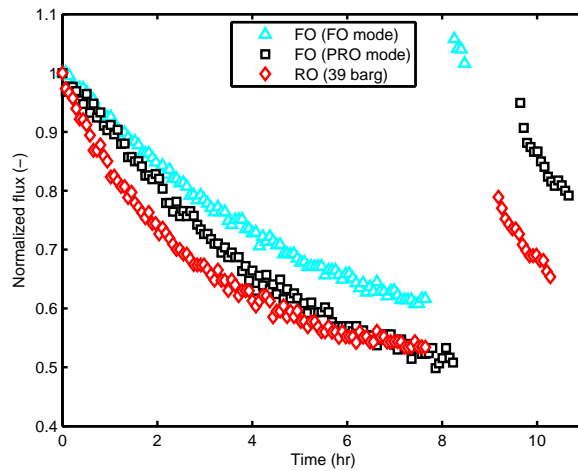
Figure 15: Flux decline and recovery in FO and RO: FO in FO mode with 4.8 M draw at 25.1 lmh initial flux, FO in PRO mode with 4.1 M NaCl draw and 23.6 lmh initial flux, and RO at 39 barg feed pressure with 21.9 lmh initial flux. Identical feed solutions of 0.17 M NaCl, 1 mM $CaCl_2$, and 200 mg/L alginate are used. Cleaning was performed with reverse flux in all trials, but for only 15 minutes in the FO-mode FO trial because it had already achieved complete foulant removal. Uncertainty in normalized flux is ±0.054 for FO and ±0.036 for RO.

Gas or vapor may accumulate in FO membranes due to pressure drop through the foulant or pressure drop across the solution–active layer interfaces. The buildup of a foulant cake with a fine pore structure causes a pressure drop through the cake when water permeates through it, resulting in a sub-atmospheric pressure at the FO membrane [9]. In cases where the membrane is in FO mode and the pores of the foulant cake are very fine, hydrophilic, and free of defects, the pressure can get very low or even negative in the absolute sense–that is, the water inside the cake could be in tension–without nucleating bubbles of air or water vapor because of the small size (in nanometers) of the available nucleation sites in the gel or active layer [9]. In real foulant cakes, defects may be present that are large enough to allow nucleation of dissolved air or, at lower pressures, water vapor inside the cake or at the cake-membrane interface. In PRO mode, nucleation could occur in the micrometer-scale pores in the feed-facing support layer. In a study by Wang et al. [7], optical microscope images of the support layer of HTI's CTA FO membranes show pores of roughly 10-50 μm in diameter, and SEM images appear to show some pores that are closed. The closed pores will not fill with foulant, and could allow the formation of stable

air bubbles at only slightly subatmospheric pressures (e.g., roughly -0.14 barg in 20 μm-diameter pores[4]). Therefore, the pressure drop across the foulant may be sufficient to cause vapor formation in the support layer in PRO mode.

Alternatively, the vapor phase may appear due to a pressure drop across the solution–active layer interface on both sides of the active layer, which is predicted by an osmotic pore flow model for semipermeable membranes [26]. To maintain thermodynamic equilibrium across the entrance to pores in the active layer (which have been shown to exist at diameters of 0.4-0.58 nm in RO membrane active layers by multiple positron annihilation spectroscopy studies [27]), the osmotic pore flow model of Anderson and Malone [26] predicts that the pressure inside the pores drops to approximately the hydraulic pressure minus the osmotic pressure outside the membrane. In PRO orientation, the active layer can contact solutions with osmotic pressures in the hundreds of bars, possibly resulting in highly negative pressures inside the active layer that may be low enough to generate stable vapor bubbles inside nanometer-scale pores. Based on the osmotic pore flow model and the draw solution, pressure, and temperature used in the PRO test reported here, a stable vapor phase could form in internal spaces with diameters as low as 8 nm diameter near the draw side of the active layer. This mechanism of internal vapor formation has the potential to occur regardless of foulant accumulation outside the membrane.

Despite the appearance of internal vapor formation during fouling in PRO mode, the subsequent cleaning process appears to proceed similarly to the other trials in this study. A video of the fouled PRO-mode FO membrane during cleaning is provided in the supplementary materials, and highlights are shown in Fig. 16. This cleaning step is performed with reverse flux. Initially, the textured patches disappear, which should occur when the permeation direction is reversed because the pressure in the support layer rises to atmospheric, causing vapor to condense and trapped air to shrink according to the ideal gas law. After several minutes, the entire gel sheet becomes detached

---

[4]Pressure estimate assumes feed water is saturated with dissolved air, air bubbles are spherical with diameters (confined by the pore) up to 20 μm, and water-air surface tension of 70 mN/m.
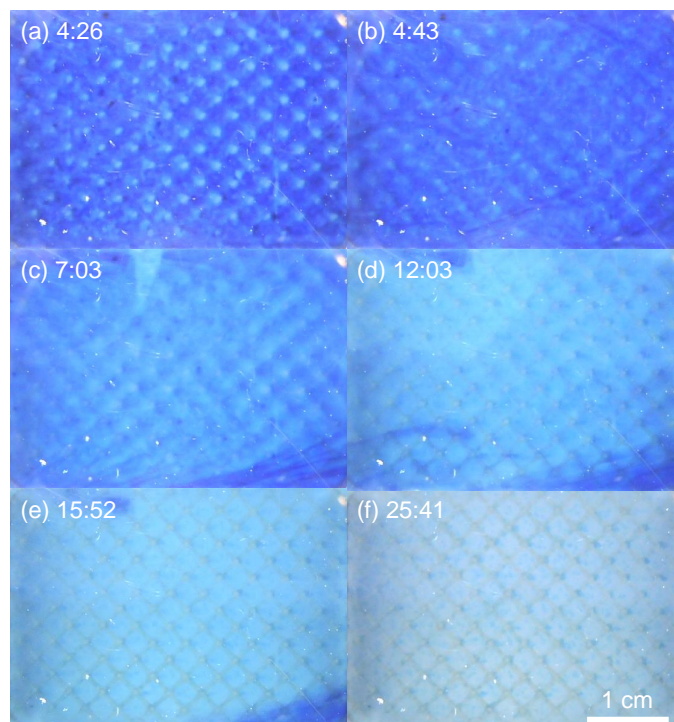
Figure 16: Video stills of cleaning the PRO-mode FO membrane shown in Fig. 14d-f. (a) After deionized water is introduced into the draw channel to reverse the direction of flow, the textured patches seen in Fig. 14 disappear. (b) The gel sheet detaches in the center and flaps in the flow. (c) The sheet rips. (d-e) Pieces of gel tear away. (f) The clean membrane.

from the membrane except at the edges, and the sheet flaps in the cross-flow and is gradually torn apart. As shown in Fig. 15, flux recovery in PRO mode was substantial but not complete. The visual record of the cleaning process (Fig. 16 and video) appears to show complete foulant removal, at least in the visible section of membrane, but the incomplete flux recovery could indicate that the internal vapor formation resulted in irreversible damage to the membrane.

5. Conclusion

In this study, mechanisms of alginate gel fouling and cleaning in RO and FO were studied using methylene blue dye in a high-pressure membrane fouling visualization module. Methylene blue was effective in that it did not affect fouling rate or cleaning effectiveness, but it only preferentially stained the foulant in low-salinity feeds ($\leq$1% wt. NaCl).

Centimeter-scale visualization of alginate fouling and cleaning revealed several mechanisms of foulant removal that were common to RO and FO:

- When cleaning alginate fouling with high cross-flow velocity, foulant removal occurs by break-away of macroscopic chunks.

- Swelling and wrinkling of the alginate gel sheet due to locally changing ionic composition are powerful mechanisms of gel detachment and may contribute to the effectiveness of osmotic backwashing.

- Although feed spacers reduce the rate of fouling, they also hinder cleaning by preventing pieces of detached gel from flowing downstream.

Additionally, one internal fouling mechanism was identified that is unique to FO membranes: vapor phase formation within the membrane.

Understanding these mechanisms is a step toward predictive modeling of the effectiveness of cleaning processes and better design of membranes, spacers, and cleaning cycles for long-term control of membrane fouling in desalination systems.

6. Acknowledgment

References

[1] M. T. Khan, M. Busch, V. G. Molina, A.-H. Emwas, C. Aubry, J.-P. Croue, How different is the composition of the fouling layer of wastewater reuse and seawater desalination RO membranes?, Water Research 59 (2014) 271 – 282.

[2] Y. Ye, P. L. Clech, V. Chen, A. Fane, B. Jefferson, Fouling mechanisms of alginate solutions as model extracellular polymeric substances, Desalination 175 (2005) 7–20.

[3] A. P. Mairal, A. R. Greenberg, W. B. Krantz, L. J. Bond, Real-time measurement of inorganic fouling of RO desalination membranes using ultrasonic time-domain reflectometry, Journal of Membrane Science 159 (1999) 185 – 196.

[4] J. Li, V. Y. Hallbauer-Zadorozhnaya, D. K. Hallbauer, R. D. Sanderson, Cake-layer deposition, growth, and compressibility during microfiltration measured and modeled using a noninvasive ultrasonic technique, Industrial & engineering chemistry research 41 (2002) 4106–4115.

[5] H. Li, A. Fane, H. Coster, S. Vigneswaran, Direct observation of particle deposition on the membrane surface during crossflow microfiltration, Journal of Membrane Science 149 (1998) 83 – 97.

[6] J. Thompson, N. Lin, E. Lyster, R. Arbel, T. Knoell, J. Gilron, Y. Cohen, RO membrane mineral scaling in the presence of a biofilm, Journal of Membrane Science 415-416 (2012) 181 – 191.

[7] Y. Wang, F. Wicaksana, C. Y. Tang, A. G. Fane, Direct microscopic observation of forward osmosis membrane fouling, Environmental Science & Technology 44 (2010) 7102–7109.

[8] M. Xie, J. Lee, L. D. Nghiem, M. Elimelech, Role of pressure in organic fouling in forward osmosis and reverse osmosis, Journal of Membrane Science 493 (2015) 748–754.

[9] E. W. Tow, J. H. Lienhard V, Quantifying osmotic membrane fouling to enable comparisons across diverse processes, Journal of Membrane Science 511 (2016) 92 – 107.

[10] O. Smidsrod, Molecular basis for some physical properties of alginates in the gel state, Faraday Discussions of the Chemical Society 57 (1974) 263–274.

[11] E. R. Morris, D. A. Rees, D. Thom, J. Boyd, Chiroptical and stoichiometric evidence of a specific, primary dimerisation process in alginate gelation, Carbohydrate Research 66 (1978) 145 – 154.

[12] I. Braccini, S. Perez, Molecular basis of Ca2+-induced gelation in alginates and pectins: The egg-box model revisited, Biomacromolecules 2 (2001) 1089–1096.

[13] E. M. V. Hoek, M. Elimelech, Cake-enhanced concentration polarization: A new fouling mechanism for salt-rejecting membranes, Environmental Science and Technology 37 (2003) 5581–5588.

[14] R. Robinson, R. Stokes, Electrolyte Solutions: Second Revised Edition, Dover Publications, Incorporated, 2012.

[15] S. Lee, C. Boo, M. Elimelech, S. Hong, Comparison of fouling behavior in forward osmosis (FO) and reverse osmosis (RO), Journal of Membrane Science 365 (2010) 34 – 39.

[16] A. Karabelas, D. Sioutopoulos, New insights into organic gel fouling of reverse osmosis desalination membranes, Desalination 368 (2015) 114 – 126.

[17] Q. Wang, X. Zhao, A three-dimensional phase diagram of growth-induced surface instabilities, Scientific Reports 5 (2015) 8887.

[18] S. T. Moe, G. Skjaak-Braek, A. Elgsaeter, O. Smidsrod, Swelling of covalently crosslinked alginate gels: influence of ionic solutes and nonpolar solvents, Macromolecules 26 (1993) 3589–3597.

[19] S. Lee, M. Elimelech, Salt cleaning of organic-fouled reverse osmosis membranes, Water Research 41 (2007) 1134 – 1142.

[20] C. Kim, S. Lee, S. Hong, Application of osmotic backwashing in forward osmosis: mechanisms and factors involved, Desalination and Water Treatment 43 (2012) 314–322.

[21] B. Mi, M. Elimelech, Organic fouling of forward osmosis membranes: Fouling reversibility and cleaning without chemical reagents, Journal of Membrane Science 348 (2010) 337 – 345.

[22] R. K. McGovern, J. P. Mizerak, S. M. Zubair, J. H. Lienhard V, Three dimensionless parameters influencing the optimal membrane orientation for forward osmosis, Journal of Membrane Science 458 (2014) 104 – 110.

[23] N. Y. Yip, A. Tiraferri, W. A. Phillip, J. D. Schiffman, M. Elimelech, High performance thin-film composite forward osmosis membrane, Environmental Science & Technology 44 (2010) 3812–3818.

[24] Q. She, R. Wang, A. G. Fane, C. Y. Tang, Membrane fouling in osmotically driven membrane processes: A review, Journal of Membrane Science 499 (2016) 201 – 233.

[25] C. Y. Tang, Q. She, W. C. Lay, R. Wang, A. G. Fane, Coupled effects of internal concentration polarization and fouling on flux behavior of forward osmosis membranes during humic acid filtration, Journal of Membrane

Science 354 (2010) 123 – 133.

[26] J. L. Anderson, D. M. Malone, Mechanism of osmotic flow in porous membranes, Biophysical Journal 14 (1974) 957 – 982.

[27] T. Fujioka, N. Oshima, R. Suzuki, W. E. Price, L. D. Nghiem, Probing the internal structure of reverse osmosis membranes by positron annihilation spectroscopy: Gaining more insight into the transport of water and small solutes, Journal of Membrane Science 486 (2015) 106 – 118.

Appendix A. Cake structural parameter quantification method

To quantify the actual accumulation of foulant on the membrane in the evaluation of methylene blue dye and separate out the effects of varying RO membrane permeability, the structural parameter of the foulant layer is calculated using the method outlined in our previous report [9]. The fouled RO membranes are treated as a series of parallel layers through which salt and water transport can be modeled. Both hydraulic resistance and cake-enhanced osmotic pressure (see [13]) are considered. Although this method was validated for higher NaCl concentrations (≥ 0.35 M) than considered here, alginate gel pore size was calculated (and the quantification method is theoretically applicable) across a wide salinity range. For the calcium and sodium ion concentrations of the feed solutions considered herein, the alginate gel pore size can be estimated as 10.2 nm from a linear fit of the pore size measurements in [9]. With this estimate of pore size, the method described in [9] can be used to translate flux decline into an effective foulant cake thickness analogous to the structural parameter of the support layers of FO membranes:

$$S \equiv \frac{\delta \tau}{\epsilon}. \qquad (A.1)$$

Here, S is the cake structural parameter, δ is the cake thickness, τ is the cake tortuosity, and ϵ is the cake porosity. Because alginate gels are highly hydrated, they tend to have porosity and tortuosity close to one [16]. In the limit of $\tau/\epsilon \to 1$, diffusion through the gel proceeds as if through a slab of still water and the cake structural parameter can be thought of as a proxy for gel thickness.

Uncertainty in cake structural parameter in RO is based on uncertainty in foulant cake pore size as well as measured flux. Using the same method of propagation of uncertainty outlined for this experimental apparatus in [9] and assuming an uncertainty of 10% in cake structural parameter due to uncertainty in cake pore size, the 95% confidence interval in RO cake structural parameter for the present experiments starts small and rises to roughly $\pm 60\,\mu$m by the end of the experiments.